ChemComm

COMMUNICATION

View Article Online
View Journal

Cite this: DOI: 10.1039/d0cc01598a

Received 1st March 2020,
Accepted 29th April 2020

DOI: 10.1039/d0cc01598a

rsc.li/chemcomm

A H_2O_2-free electrochemical peptide biosensor based on Au@Pt bimetallic nanorods for highly sensitive sensing of matrix metalloproteinase 2†

Xiaoxue Xi, Meiqi Wen, Shihao Song, Junlun Zhu, Wei Wen,* Xiuhua Zhang and Shengfu Wang*

Inspired by the excellent catalytic activity of Au@Pt bimetallic nanorods, we construct a H_2O_2-free electrochemical peptide biosensor based on Au@Pt bimetallic nanorods for highly efficient and sensitive sensing of MMP-2 for the first time, not only simplifying the traditional testing steps but also avoiding the potential damage caused by H_2O_2 to peptides and proteins.

Electrochemical biosensors (EBs) have received particular attention in many fields owing to their advantages of high-sensitivity, fast-response and convenience of operation.[1] The exploration and development of high-efficiency EBs for sensitive detection of biomarkers is urgent to meet the ever-increasing demands of people for health care services in the modern society. In fact, many efforts have been undertaken and different signal amplification methods have been put forward to improve the sensitivity of EBs, such as hybridization chain reactions (HCRs),[2] rolling circle amplification,[3] and enzyme-catalyzed amplification.[4] Among them, enzyme-labeled EBs have attracted considerable interest due to the excellent reactivity, selectivity and catalytic activity of enzymes towards substrates. However, due to the difficult separation and high cost of enzymes, although vast endeavors have been made to immobilize enzymes using nanomaterials to address these limitations,[5] the undesired activity loss of enzymes after a series of cumbersome and necessary conjugation processes is really nonnegligible. Therefore, it is necessary to develop a new type of amplification strategy to solve the problems mentioned above from the improvement of assay performance point of view.

Nanozymes possess many inherent superiorities compared with natural enzymes, including excellent stability, ease of separation, low-cost preparation and high resistance to acids or alkalis,[6] and have attracted increasing interest in many fields due to their excellent affinity for biomolecules and significant signal amplification effect, paving a new path for the exploration of nanozymes as biolabels. Up to now, four kinds of redox enzymes have been mimicked by nanomaterials, including catalases,[7] peroxidases,[8] oxidases,[9] and superoxide dismutases.[10] Wei's group synthesized fluorescent graphitic carbon nitride (C_3N_4)-based nanomaterials with superior peroxidase-like activity and constructed a novel platform for sensitive sensing of H_2O_2 and glucose.[11] Qu's group synthesized a type of doped graphene oxide and gold nanocluster with excellent peroxidase-like activity and fabricated a convenient, cheap colorimetric platform for sensitive detection of cancer cells.[12] In our previous studies, an array of nanozymes with superior peroxidase-like activities and photothermal effects have also been synthesized, such as CuO-g-C_3N_4 nanosheets, hollow CuS nanocubes and metal doped g-C_3N_4 nanoflakes exhibiting excellent affinity toward traditional H_2O_2–TMB systems, and applied in the colorimetric detection of H_2O_2 and dopamine.[13,14] However, they all rely on the addition of external oxidants, like H_2O_2 or acidic substrate solutions (pH = 3–4). This not only caused unnecessary decomposition during the storage process but also brought about inevitable damage to some analytical targets, including peptides and proteins, on account of the unstable properties and strong oxidizing properties of H_2O_2.[15] In addition, the involvement of H_2O_2 makes the experimental steps complicated and labor-consuming, as with the common conventional TMB-H_2O_2 system, and the two liquid solutions are usually stored individually due to their unstable performances and then mixed together when needed,[16] which may introduce inevitable assay errors in the experiments and increase the operational complexities of detection. In regard of this, introducing a kind of nanozyme-based signal label to set up a reliable H_2O_2-free electrochemical biosensor in neutral solution to address these limitations is really attractive and desirable.

Peptides are compounds formed by the dehydration condensation of 10–100 natural amino acid molecules as building blocks *via* peptide bonds. They are prominent candidates for constructing biosensors with high sensitivity and convenience, ascribed to their specific identification sequences, remarkable

State Key Laboratory of Biocatalysis and Enzyme Engineering & Ministry of Education Key Laboratory for the Synthesis and Application of Organic Functional Molecules, College of Chemistry and Chemical Engineering, Hubei University, Wuhan 430062, People's Republic of China. E-mail: wenwei@hubu.edu.cn, wangsf@hubu.edu.cn

† Electronic supplementary information (ESI) available. See DOI: 10.1039/d0cc01598a

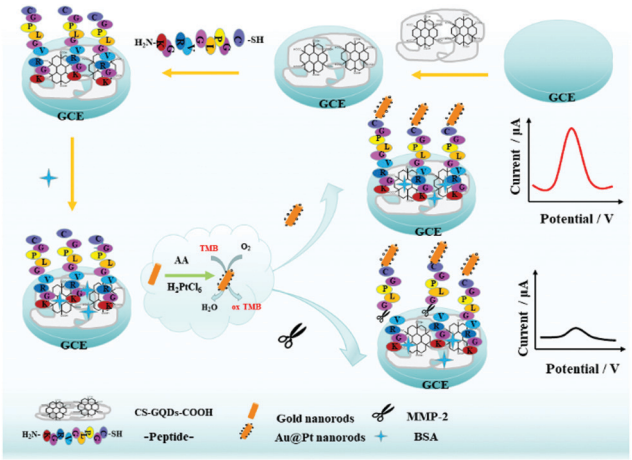

Scheme 1 Schematic illustration of the construction of a H_2O_2-free electrochemical peptide biosensor for MMP-2 assay.

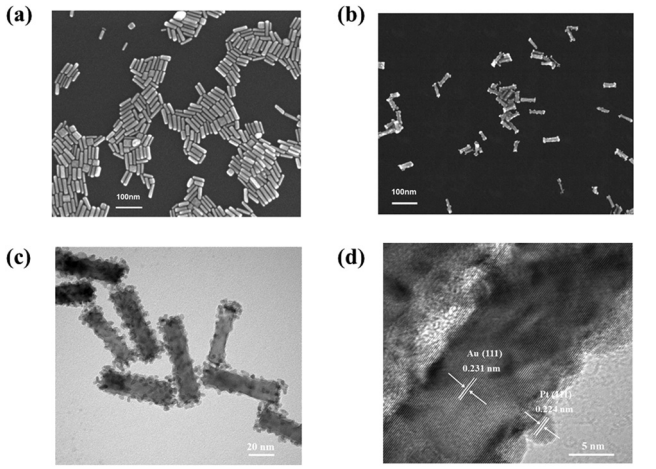

Fig. 1 The SEM images of Au NRs (a) and Au@Pt nanorods (b), TEM image (c) and HR-TEM image (d) of Au@Pt nanorods.

affinity for target detectors and easy modification.[17] For example a specific substrate sequence (–PLGVR–) can be utilized for the sensitive assaying of MMP-2,[18] which is closely related to the growth, invasion and metastasis of tumors, including breast cancer, bladder cancer and cervical cancer.[19]

In this work, we fabricated for the first time a H_2O_2-free electrochemical peptide biosensor with an Au@Pt bimetallic nanozyme as a signal amplification label for sensitive detection of MMP-2 in neutral substrate solution even with dissolved O_2 (Scheme 1). The directional design and synthesis of noble nanomaterials have been extensively explored by Li's group.[20] Here we synthesized the Au@Pt nanorods *via* a seed-mediated growth process and an *in situ* reduction method, which can enable the catalytic oxidation of 3,3′,5,5′-tetramethylbenzidine (TMB) efficiently even with dissolved O_2 due to their superior catalytic activity. Particularly interesting is that they exhibited a similar effect in comparison with the system containing H_2O_2. The peptide and Au@Pt nanorods were immobilized on the electrode by layer-by-layer assembly *via* amide reaction and Au–S bonds, and then the Au@Pt nanorods could enable the catalytic oxidation of signal molecules (TMB) efficiently even with dissolved O_2 and generate an intense DPV current response. After incubating with MMP-2, a sharply declined electrochemical signal was observed. The biosensor exhibited prominent sensitivity with a wide detection range of 0.5–100 ng mL^{-1} and the detection limit is 0.18 ng mL^{-1}. Such a novel peptide biosensor was fabricated to prevent the damage caused by H_2O_2 to peptides or proteins, holding promise for further application in biological detection and clinical diagnosis.

Transmission electron microscopy (TEM), scanning electron microscopy (SEM), energy dispersive X-ray spectroscopy (EDS), and elemental mapping (Fig. S3, ESI†) were conducted to observe the morphological features and investigate the elemental distribution of gold nanorods and Au@Pt nanorods. As shown in Fig. 1a and Fig. S2a (ESI†), the AuNRs synthesized through a seed-mediated growth method exhibited smooth clearly rods ascribed to the uniform distribution. The average length and width of the AuNRs were calculated to be 43.3 ± 4.9 nm and 11.2 ± 2.3 nm respectively (Fig. S1a and b, ESI†). The Au@Pt nanorods were obtained through *in situ* reduction methods with AuNRs as a template. The Pt nanodots were wrapped on the surface of the AuNRs homogeneously and formed a rough shell, as observed from Fig. 1b and c and Fig. S2b–d (ESI†). The average length and width were 57.9 ± 4.9 nm and 14.5 ± 2.6 nm respectively (Fig. S1c and d, ESI†). Fractional aggregation of AuNRs can be ascribed to the defects within CTAB, a lower concentration of CTAB may result in the double layers formed with CTAB being shared between two or even more AuNRs.[21] The HR-TEM image of Au@Pt nanorods (Fig. 1d) showed clear lattice distances of 0.224 nm and 0.231 nm, which can be assigned to the (111) planes of crystalline Pt and Au. The peaks at 38.3°, 44.3°, 64.9°, and 77.5° can be attributed to the (111), (200), (220) and (311) diffraction planes of Au and Pt bimetallic nanorods (Fig. S4d, ESI†), which are consistent with the HR-TEM results.[22] For the purpose of exploring the chemical valence and elemental composition of the material, high-resolution X-ray photoelectron spectroscopy (XPS) was performed subsequently. As shown in Fig. S4a (ESI†), two distinct absorption peaks at 285.1 eV and 532.8 eV can be associated with the absorbed H_2O, CO_2 molecule and partially residual surfactants. The XPS spectrum of Pt 4f is depicted in Fig. S4c (ESI†). Two apparent absorption peaks at 71.2 eV (Pt $4f_{7/2}$) and 74.9 eV (Pt $4f_{5/2}$) can be assigned to the presence of metallic Pt. Similarly, the spin split double peaks at 83.9 eV (Au $4f_{7/2}$) and 87.7 eV (Au $4f_{5/2}$) are attributed to metallic Au.[23] Ultraviolet-visible (UV-vis) spectrophotometry was also used for studying the spectral properties of Au@Pt nanorods (Fig. S5, ESI†). The absorption band exhibited an evident red-shift from 851 nm to 916 nm after loading Pt nanodots on the surface of Au nanorods, and the colour also experienced an enormous variation from wine red to dark gray. The large red-shift (65 nm) can be associated with the generation of the Pt shell composed of uniformly dispersed Pt nanodots.[24] These characteristic results confirmed the successfully synthesis of Au@Pt nanorods.

To investigate the catalytic activity of AuNRs and Au@Pt nanorods, UV-vis spectroscopy was applied to monitor the

strength of the absorbance with AuNRs and Au@Pt nanorods as catalysts. An intense blue colour and a strong absorption peak heaved into sight with Au@Pt nanorods as a catalyst (Fig. S6, ESI†), which can be ascribed to the superior bimetallic catalytic effect towards the TMB–O_2 system.

The stepwise assembly processes for the constructed biosensor were monitored by electrochemical impedance spectroscopy (EIS) in 0.1 M KCl containing 5 mM $[Fe(CN)_6]^{4-/3-}$ as a redox probe (Fig. S7, ESI†). In addition, the zeta potentials of the Au@Pt nanorods before and after modification with polypeptides were also explored (Fig. S8, ESI†). These results illustrated the successful construction of the electrochemical peptide biosensor.

The electrochemical biosensor incubated without MMP-2 exhibited an intense current response, and then the current response decreased gradually accompanied by the increasing addition of MMP-2 from 0 to 100 ng mL^{-1} (Fig. S10, ESI†). The results confirmed the excellent catalytic efficiency of the Au@Pt nanozyme and the feasibility for the following assay of MMP-2 in the absence of H_2O_2.

For the purpose of further investigating the superior catalytic properties of the Au@Pt nanorods, we fabricated an electrochemical peptide biosensor for the sensitive assay of MMP-2 with the Au NRs and Au@Pt nanorods as nanozymes, respectively. As depicted in Fig. 2a and b, the EBs based on the Au@Pt nanorods exhibited superior catalytic activity towards the signal molecule (TMB). The value of ΔI is 7.11 μA (the value of ΔI is calculated using $\Delta I = I_n - I_0$, where I_n represents the blank signals of the biosensor with 0 ng mL^{-1} MMP-2, while I_0 represents the signals of the biosensor incubated with MMP-2), which is much higher than that of Au NRs (ΔI = 3.7 μA). The excellent catalytic properties can be associated with the superior catalytic activity of the two noble metals. What's more interesting is that the system can operate even with dissolved O_2 displaying a similar DPV response value compared with the system involving H_2O_2 (ΔI = 7.22 μA) (Fig. 2c). Besides, we also found that the DPV response is not stable for the system involving H_2O_2, and the DPV current had dropped significantly during the second round of consecutive scanning, while the system only with dissolved O_2 displayed a stable DPV current response even after two rounds of scanning (Fig. S11, ESI†). These results further proved that H_2O_2 exhibited a certain possible potential effect on proteins and influenced the stability of electrochemical peptide biosensors. In order to demonstrate the importance of dissolved O_2 in the system, we introduce N_2 to remove the O_2 dissolved in the solution and create an O_2-free environment for the whole system. As depicted in Fig. 2d, the electrochemical signal showed a sudden drop in the anaerobic environment and then the current response recovered subsequently after saturation with the O_2 of the substrate solution. The results well illustrated that dissolved O_2 plays a pivotal role in the fabrication of a H_2O_2-free electrochemical peptide biosensor, and the possible catalytic mechanism is also discussed in the ESI.†

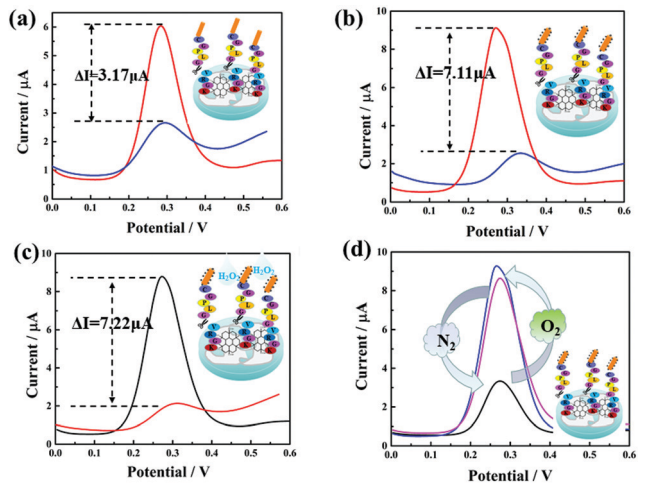

Fig. 2 Comparison of the DPV response curves of the biosensor and different nanoprobes: AuNRs(a) and Au@Pt nanorods (b). The biosensor was measured in 3 mL PBS (10 mM, pH = 7.4) containing 100 μL TMB (10 mM) in the absence (red line) and presence (blue line) of 100 ng mL^{-1} MMP-2; the DPV comparison between the biosensor without H_2O_2 (b) and with H_2O_2 (c). The biosensor was measured in the absence (black line) and presence (red line) of 100 ng mL^{-1} MMP-2; (d) the DPV curves of the detection solution only with dissolved O_2 (red line), with saturated N_2 (black line) and with saturated O_2 (blue line).

For the purpose of achieving the best assay performance and maximizing the sensing sensitivity, an array of experimental parameters were optimized, including the concentration of the polypeptide, the incubation time of MMP-2 and the volume of TMB. As depicted in Fig. S12 (ESI†), the DPV current response enhanced with the increasing concentrations of the peptide and the maximum current response value was observed when the concentration reached 10 μM. Similarly, an obvious plateau was observed when the incubation time of MMP-2 was up to 60 min and the volume of TMB reached 100 μL (Fig. S13 and 14, ESI†). Therefore we finally selected 20 μM polypeptide, 60 min incubation time for MMP-2, and 100 μL TMB (10 mM) as the optimal culture conditions for the subsequent experiments.

Using the optimal experimental parameters, we explored the sensitivity of the biosensor for detection of MMP-2. As demonstrated in Fig. 3a, the DPV current response decreased gradually along with the increasing concentrations of MMP-2, from 0 to 100 ng mL^{-1}. A good linear correlation was observed between the changes in the DPV response value ΔI and the logarithm of MMP-2 concentrations from 0.5 to 100 ng mL^{-1} using the linear equation of ΔI (μA) = 2.935lgC (ng mL^{-1}) + 0.963 (R^2 = 0.994), and the limit of detection (LOD = $3\sigma/k$) was calculated as 0.18 ng mL^{-1} (Fig. 3b). The assay sensitivity of our biosensor is comparable with other detection methods reported previously for sensing MMP-2 (Table S1, ESI†).

The possible interferents during the detection process were explored subsequently to evaluate the specificity of the biosensor (Fig. 3c). Several analogues of the biosensor exhibited near negligible DPV signals compared with the blank experiment; however, the signal response decreased remarkably after incubation with MMP-2. The results demonstrated the desirable selectivity of the biosensor.

For the purpose of evaluating the stability of the electrochemical biosensor, six different electrodes were cultured

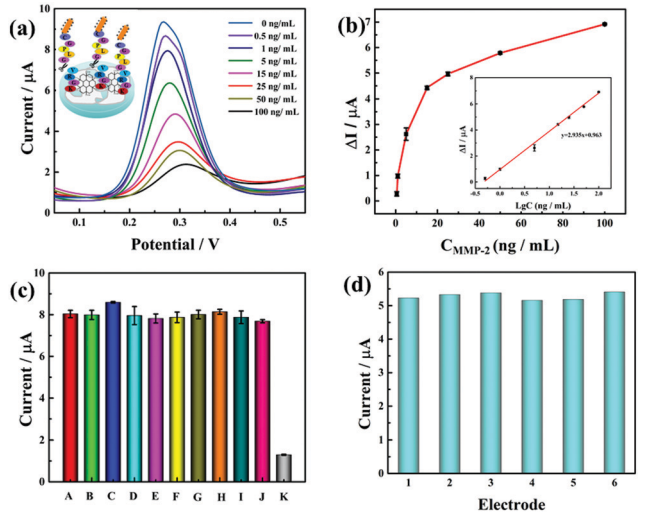

Fig. 3 (a) The DPV response curves of the fabricated biosensor incubated with various concentrations of MMP-2; (b) calibration curve of the fabricated biosensor for MMP-2 detection under optimal experimental conditions. (c) Comparison of DPV responses of the biosensor for the assay of MMP-2 (100 ng mL^{-1}) with potential interferents: A to K are blank, Fe^{3+}, Cu^{2+}, PSA, glucose, bovine serum albumin, human serum albumin, thrombin, arginine, glutamate. (d) Reproducibility test of six independently prepared peptide-based electrochemical biosensors for detecting 10 ng mL^{-1} MMP-2.

under the same conditions and the corresponding DPV responses were recorded. As demonstrated in Fig. 3d, the six electrodes showed almost similar DPV response values, which further suggests that the biosensor we designed showed an enviable and satisfactory reproductivity.

In addition, for the purpose of exploring the practicability and feasibility of our biosensor, recovery experiments were carried out by adding three different concentrations of MMP-2 into the 100-fold diluted human serum. As depicted in Table S2 (ESI†), upon adding different concentrations of MMP-2, the recoveries always range from 96.1 to 104.4% and the relative standard deviation (RSD) ranges from 1.2% to 4.8%. What's more, the whole experiment was performed in neutral substrate solutions (pH = 7.4) without any unstable H_2O_2 substrate, and these results all proved that the electrochemical peptide biosensor we proposed has enormous potential for the assay of MMP-2 in complex practical biological samples in the future.

In summary, a H_2O_2-free electrochemical peptide biosensor for sensitive sensing of MMP-2 using Au@Pt nanorods in neutral substrate solutions even with dissolved O_2 was constructed for the first time. The Au@Pt nanoparticles exhibited an excellent catalytic activity towards TMB even without the presence of H_2O_2. The peptide-based biosensor contains several inherent merits: (i) The highly reliable electrochemical biosensor can operate even with dissolved O_2, avoiding the involvement of any strongly oxidized substrate of H_2O_2, which greatly simplified the operation steps and avoided potential damage to proteins or peptides. (ii) Neutral substrate solutions (pH = 7.4) were applied for the biosensor; the avoidance of acidic test solutions further expanded its practical application in biological samples. (iii) TMB was used as the electrochemical signal molecule, which eliminates the tedious labelling process. In other words, the H_2O_2-free peptide biosensor can be applied to detect an array of target biomolecules by changing the sequence of peptides and has enormous potential for application in disease diagnosis and biomedical research.

This work was supported by the National Natural Science Foundation of China (No. 21405035 and 21775033) and the Open Project Funding of the State Key Laboratory of Biocatalysis and Enzyme Engineering.

Conflicts of interest

There are no conflicts to declare.

Notes and references

1 N. Wongkaew, M. Simsek, C. Griesche and A. J. Baeumner, *Chem. Rev.*, 2018, **119**, 120–194.
2 Z. L. Ge, M. H. Lin, P. Wang, H. Pei, J. Yan, J. Y. Shi, Q. Huamg, C. H. Fang and X. L. Zuo, *Anal. Chem.*, 2014, **86**, 2124–2130.
3 Y. Q. Cheng, X. Zhang, Z. P. Li, X. X. Jiao, Y. C. Wang and Y. L. Zhang, *Angew. Chem., Int. Ed.*, 2009, **48**, 3268–3272.
4 B. Li, G. S. Lai, B. Lin, A. M. Yu and N. J. Yang, *Sens. Actuators, B*, 2018, **262**, 789–795.
5 Y. D. Liu, X. H. Liu, Z. P. Guo, Z. G. Hu, Z. H. Xue and X. Q. Lu, *Biosens. Bioelectron.*, 2017, **87**, 101–107.
6 J. J. Wu, X. Y. Wang, Q. Wang, Z. P. Lou, S. R. Li, Y. Y. Zhu, L. Qin and H. Wei, *Chem. Soc. Rev.*, 2019, **48**, 1004–1076.
7 C. P. Liu, T. H. Wu, C. Y. Liu, K. C. Chen, Y. X. Chen, G. S. Chen and S. Y. Lin, *Small*, 2017, **13**, 1700278.
8 F. Attar, M. G. Shahpar, B. Rasti, M. Sharifi, A. A. Saboury, S. M. Rezayat and M. Falahati, *J. Mol. Liq.*, 2019, **278**, 130–144.
9 M. C. Ortega-Liebana, J. L. Hueso, R. Arenal and J. Santamaria, *Nanoscale*, 2017, **9**, 1787–1792.
10 A. S. Jalilov, L. G. Nilewski, V. Berka, C. H. Zhang, A. A. Yakovenko, G. Wu, T. A. Kent, A. L. Tsai and J. M. Tour, *ACS Nano*, 2017, **11**, 2024–2032.
11 X. Y. Wang, L. Qin, M. J. Lin, H. Xing and H. Wei, *Anal. Chem.*, 2019, **91**, 10648–10656.
12 Y. Tao, Y. H. Lin, Z. Z. Huang, J. S. Ren and X. G. Qu, *Adv. Mater.*, 2013, **25**, 2594–2599.
13 J. L. Zhu, W. Nie, Q. Wang, J. W. Li, H. Li, W. Wen, T. Bao, H. Y. Xiong, X. H. Zhang and S. F. Wang, *Carbon*, 2018, **129**, 29–37.
14 J. L. Zhu, X. Peng, W. Wen, X. H. Zhang and S. F. Wang, *Biosens. Bioelectron.*, 2019, **141**, 111450.
15 T. Nakayama, *Cancer Res.*, 1994, **54**, 1991s–1993s.
16 L. Jiao, W. Q. Xu, H. Y. Yan, Y. Wu, W. L. Gu, H. Li, D. Du, Y. H. Lin and C. Z. Zhu, *Chem. Commun.*, 2019, **55**, 9865–9868.
17 L. C. Szymczak, H. Y. Kuo and M. Mrksich, *Anal. Chem.*, 2017, **90**, 266–282.
18 B. B. Kou, Y. Q. Chai, Y. L. Yuan and R. Yuan, *Anal. Chem.*, 2017, **89**, 9383–9387.
19 M. M. Shi, B. Yu, H. G. Gao, J. W. Mu and C. W. Ji, *Mol. Biol. Rep.*, 2013, **40**, 617–623.
20 C. L. Li, M. lqbal, B. Jiang, Z. L. Wang, J. Kim, A. E. Whitten and Y. Yamanchi, *Chem. Sci.*, 2019, **10**, 4054–4061.
21 R. Becker and P. O. Käll, *J. Colloid Interface Sci.*, 2010, **343**, 25–30.
22 L. Wang, B. Qi, C. L. Guo and Z. Li, *Mater. Lett.*, 2008, **62**, 1279–1282.
23 B. Y. Xia, H. B. Wu, N. Li, Y. Yan, X. W. Lou and X. Wang, *Angew. Chem., Int. Ed.*, 2015, **54**, 3797–3801.
24 W. W. He, Y. Liu, J. S. Yuan, J. J. Yin, X. C. Wu, X. N. Hu, K. Zhang, J. B. Liu, C. Y. Chen, Y. L. Ji and Y. T. Guo, *Biomaterials*, 2011, **32**, 1139–1147.

